

Deflickering Vision-Based Occupancy Networks through Lightweight Spatio-Temporal Correlation

Fengcheng Yu, Haoran Xu, Canming Xia, Ziyang Zong, and Guang Tan

Abstract—Vision-based occupancy networks (VONs) provide an end-to-end solution for reconstructing 3D environments in autonomous driving. However, existing methods often suffer from temporal inconsistencies, manifesting as flickering effects that compromise visual experience and adversely affect decision-making. While recent approaches have incorporated historical data to mitigate the issue, they often incur high computational costs and may introduce noisy information that interferes with object detection. We propose OccLinker, a novel plugin framework designed to seamlessly integrate with existing VONs for boosting performance. Our method efficiently consolidates historical static and motion cues, learns sparse latent correlations with current features through a dual cross-attention mechanism, and produces correction occupancy components to refine the base network’s predictions. We propose a new temporal consistency metric to quantitatively identify flickering effects. Extensive experiments on two benchmark datasets demonstrate that our method delivers superior performance with negligible computational overhead, while effectively eliminating flickering artifacts.

Index Terms—vision-based occupancy network, deflickering, spatio-temporal correlation, plug-and-play.

I. INTRODUCTION

Vision-based Occupancy Networks (VONs) [1]–[6] have emerged as a powerful paradigm for reconstructing surrounding environments from ego-centric multi-view images. Typically, VONs represent the scene as a structured grid of voxels [7] by learning accurate mappings from 2D visual cues to 3D occupancy representations. This approach enables the extraction of both geometric structure and semantic understanding, thereby facilitating various applications, including indoor navigation [8], [9] and autonomous driving [5], [10]–[12].

Despite these progresses, the occupancy results generated by existing VONs often exhibit inaccuracies and visual imperfections. A particularly problematic phenomenon, which we term **flickering**, manifests as instability in the constructed scenes: objects may appear or disappear abruptly, accompanied by various artifacts. This lack of temporal consistency and accuracy not only confuses the driving control system but also seriously degrades the visual experience for human drivers. The primary causes of flickering include sensor noise, occlusion, model limitations, and thresholding issues. As illustrated in Fig. 1,

The authors are with Sun Yat-sen University, Shenzhen 518107, China. (e-mail: fyu54107@usc.edu, {xuhr9, xiacm, zongzy}@mail2.sysu.edu.cn, tan-guang@mail.sysu.edu.cn)

Haoran Xu and Canming Xia are also with the Department of Intelligent Computing, Peng Cheng Laboratory, Shenzhen 518066, China.

Fengcheng Yu and Haoran Xu contributed equally to the paper.

Corresponding author: Guang Tan

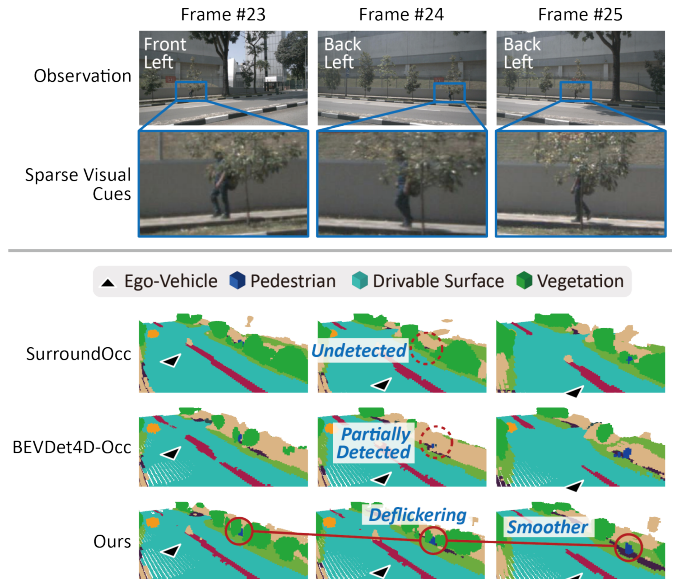


Fig. 1: Enhancing existing VONs with OccLinker. (i) In the upper part, the first row shows three consecutive images where the ego-vehicle moves forward along the right side of the road. The blue box highlights a pedestrian as a sparse visual cue, and the second row provides the corresponding zoomed-in views. (ii) In the lower part, we compare different types of VON methods. The first row shows a standard 3D VON [13] that ignores historical information, resulting in the pedestrian being missed in certain frames. The second row presents a history-aware VON [14] that utilizes past frames but still produces incomplete voxels due to suboptimal temporal association. In contrast, our module, when integrated with the 3D VON [13], achieves smoother and more complete occupancy predictions through effective spatio-temporal correlation.

a pedestrian occluded by a tree provides incomplete visual cues, posing a significant challenge to the prediction models. In this case, SurroundOcc [13], which operates in a frame-by-frame “detection” paradigm, fails to detect the pedestrian in Frame #24. The temporary absence of the person will create a flickering effect when the results are displayed to the user.

An effective approach to mitigate the temporal inconsistency problem is to incorporate historical information when predicting the current occupancy. Recent history-aware VONs [14]–[17] have explored this direction and can be broadly categorized into two classes: dense Bird’s Eye View (BEV)/voxel-based temporal fusion methods and sparse query or representation based methods. Specifically:

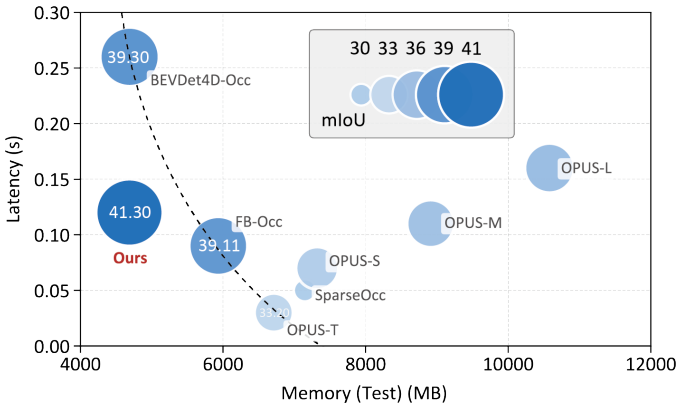


Fig. 2: Comparison with history-aware VON methods in terms of mIoU and running costs. Points closer to the bottom-left indicate better efficiency, with lower memory usage and faster inference. Larger circles denote higher prediction quality with mIoU shown in numbers. Our method, when integrated with ViewFormer, achieves the best mIoU and the lowest memory consumption, while maintaining competitive inference latency.

- **Dense methods** [14], [17]–[22] perform dense temporal modeling, typically by propagating, aligning, or aggregating historical BEV features or volumetric representations into the current frame. These approaches incur substantial computational and memory costs, often limiting the feasible temporal window or spatial resolution. For example, as shown in Fig. 2, BEVDet4D-Occ produces the largest inference latency. Moreover, dense temporal aggregation may propagate redundant or noisy features across broad spatial regions, leading to unstable predictions in dynamic areas. As illustrated in the lower part of Fig. 1, the pedestrian appears unclear in the BEVDet4D-Occ results, likely due to coarse-grained temporal fusion.
- **Sparse methods** seek to reduce the complexity of dense voxel fusion by operating on sparse queries [15], [23] or representations [16], [24], [25]. By focusing computation on most relevant latent regions, methods such as SparseOcc and the OPUS series typically achieve lower inference latency (see Fig. 2). These methods often require multi-stage recovery or decoding processes to reconstruct dense occupancy. For instance, SparseOcc employs diffusion-based propagation combined with feature pyramids to densify non-empty regions across scales, whereas OPUS adopts a coarse-to-fine cross-attention mechanism to progressively decode sparse queries into 3D space. These designs increase memory usage and produce of reduced voxel-level accuracy.

Different from existing methods, we explore an alternative approach: enhancing temporal consistency through a lightweight plug-in module that leverages historical information without redesigning the backbone, altering the fusion strategy, or retraining the base VON from scratch. Specifically, our approach only requires training a lightweight module on top of existing VON predictions or intermediate features, making it both practical and broadly applicable.

To this end, we propose a novel method, termed **OccLinker**.

Our approach improves occupancy prediction by discriminating and extracting relevant motion and static cues from historical frames, emphasizing *lightweight yet effective* spatio-temporal correlation modeling. OccLinker follows a three-stage framework. First, it converts historical static and motion cues into queries through sparse tokenization. Next, an independent latent correlation module is introduced to attentively associate current features with historical cues within a shared latent space. Finally, the system generates *correction occupancy* that enables refinement of the base network’s results. Our method offers two key advantages:

- Seamless integration with state-of-the-art (SOTA) VONs for significantly enhanced prediction accuracy. When integrated with SurroundOcc [13] on its benchmark, it elevates IoU and temporal consistency of moving objects (as defined in the Experiment section) by 1.63% and 2.31, respectively. Similarly, when combined with ViewFormer [17] on the Occ3D [7] benchmark, it achieves gains of 0.24% in IoU and 2.87 in temporal consistency;
- Low cost through lightweight correlation operation, which surpasses recent history-aware VONs [14], [15], [18] with much lower computational costs. For instance, OPUS-L [15] requires 10.33 GB of GPU memory and 0.16 seconds per frame for inference. In contrast, ViewFormer+OccLinker only needs 4.58 GB memory and 0.12 seconds. Notably, the OccLinker plug-in itself uses just 105 MB of memory and adds only 0.01 seconds of latency.

These two advantages jointly push our method beyond the usual accuracy-efficiency Pareto frontier. As illustrated in Fig. 2, existing history-aware approaches demonstrate a clear trade-off between performance and cost. In contrast, our method, when combined with ViewFormer, achieves superior accuracy without sacrificing efficiency.

In summary, the contributions of this paper are three-fold:

- We introduce OccLinker, a parameter-efficient plug-in that integrates seamlessly with existing 3D VONs without requiring any modifications to the base network. It incurs only minimal GPU memory overhead and negligible inference latency, while consistently enhancing prediction accuracy.
- We propose a lightweight spatio-temporal correlation learning method that effectively fuses historical cues, sparse motion features, as well as current static tokens. These cues are mapped into a shared compact latent space, enabling pixel-to-voxel correlation through adaptive 3D occupancy aggregation.
- We devise a new temporal consistency metric to help analyze the effectiveness of various occupancy methods. Extensive experiments are conducted on both SurroundOcc [13] and Occ3D [7] benchmarks, showing the advantages of our approach in accuracy while maintaining real-time inference efficiency.

The remainder of this article is structured as follows: Section II reviews related work; Section III elaborates on the design of our proposed method; Section IV presents

experimental results; and Section V concludes this paper with a discussion of future work.

II. RELATED WORK

A. 3D Scene Reconstruction

3D scene reconstruction technology has evolved rapidly in autonomous driving. Early studies focused on mathematical methods [26] and camera parameters [27]–[29] to facilitate 3D scene reconstruction from 2D inputs. MonoScene [26] explored the path of scene reconstruction from 2D to 3D using monocular RGB images, setting a groundbreaking benchmark. Later, more learning methods were applied. 1) Multi-view reconstruction [30]–[32], which integrates multiple perspectives for enhanced depth estimation. 2) Multimodal methods combining RGB with depth [33], [34] or RGB with LiDAR [35] data, improving the robustness and precision of reconstructions.

B. 3D VONs

3D VONs extend the capabilities of 3D scene reconstruction technologies to enhance dynamic and precise environmental perception for autonomous vehicles. This task involves learning the associations between pixel-level visual cues and the occupancy states of 3D voxels. Recent approaches often employ Transformers [36] to effectively model these complex relationships, achieving significant advancements in accuracy and efficiency. 3D occupancy prediction have utilized multiple data inputs such as LiDAR [37]–[39] and depth data [40]–[46] to predict voxel occupancy. However, with advancements in camera technology and image processing, current research predominantly adopts an image-based end-to-end approach [3], [13], [47]–[49]. These modern methods use data from single frames to predict occupancy, focusing on integrating rich semantic information at lower costs. However, due to the high-dimensional visual input and dense grid-based output, end-to-end methods suffer from significant computational intensity. To address this, more recent works [25], [50]–[53] have incorporated Gaussian point clouds as an intermediate representation. These point clouds are projected into the 3D occupancy space using splatting techniques, which significantly reduce memory consumption.

C. History-aware VONs

Recent advances in spatio-temporal perception have extended 3D VONs into temporal domains, primarily through two paradigms: (i) 4D VONs that estimate current and future states (e.g., Cam4DOcc [54], OccSora [55]), and (ii) history-aware VONs [14]–[16], [18] leverage historical features to refine current-frame predictions. In this paper, we focus primarily on the second category, which, as discussed in the Introduction, can be further classified into dense BEV or voxel-based temporal fusion [14], [17]–[22] and sparse query [15], [23] or representation-based methods [16], [24], [25]. For instance, the sparse method OPUS [15] uses a learnable query-based encoder-decoder architecture and retains coarse-grained concatenation of raw image features during early fusion stages,

while the dense method BEVDet4D-Occ [14] performs spatio-temporal alignment from a BEV perspective. In contrast, we propose a different approach, using a lightweight plugin that effectively discriminates and extracts relevant motion-static attention, complementing the current occupancy predictions. Our method does not conflict with existing history-aware approaches and can seamlessly integrate with them or other 3D VONs to enhance both occupancy accuracy and temporal consistency.

III. METHODOLOGY

A. Problem Formulation

In the context of vision-based occupancy networks (VONs) [3], [5], [10], [12], [13] for autonomous driving, the ego-vehicle typically collects two types of data: (i) multi-view RGB frames from surround-view cameras (typically six), captured at a relatively low and fixed frequency – we refer to these as keyframes; (ii) higher-frequency motion information between keyframes, such as optical flow or frame differences.

As illustrated in Fig. 3, given a temporal window \mathcal{W} of length L , the input includes a sequence of L historical keyframes denoted by $S_{t-L:t-1}$, one current keyframe S_t , and a corresponding sequence of L motion cues $M_{t-L:t-1}$, where each motion cue represents frame differences over a short interval Δt . Let $|V|$ denote the number of cameras. For simplicity, we merge all multi-view inputs into a unified notation and do not distinguish between individual camera views. Both RGB and motion frames are assumed to have the same spatial resolution.

Typically, a base 3D VON Φ first encodes the current keyframe S_t using a 2D encoder Φ_{SE} to extract static appearance features s_t . These features are then lifted into 3D space via a 2D-to-3D decoder Φ_{SD} , resulting in an initial occupancy prediction O'_t . That is:

$$s_t = \Phi_{SE}^*(S_t), \quad O'_t = \Phi_{SD}^*(s_t), \quad (1)$$

where \cdot^* indicates frozen weights from the pre-trained foundational network. Since the base VON operates in a frame-by-frame manner, the historical static features $s_{t-L:t}$ extracted by the frozen static encoder Φ_{SE}^* are pre-stored and reused for temporal correlation modeling.

Our goal is to design a lightweight plug-in module, parameterized by Θ , that associates the motion features within a temporal window of length L with the static features $s_{t-L:t}$ extracted by the base VON, thereby enhancing the foundational prediction O'_t at each timestep t . To achieve this, the intermediate frame differences, denoted by $M_{t-L:t-1}$, is first encoded into a latent representation using a motion encoder Φ_{ME} , yielding temporal motion features:

$$m_{t-L:t-1} = \Phi_{ME}(M_{t-L:t-1}). \quad (2)$$

To enable efficient feature linking, we employ a lightweight tokenization encoder ϕ that transforms both the static features $s_{t-L:t}$ and the motion features $m_{t-L:t-1}$ into a compact sparse token set. Subsequently, the cross-attention module Θ establishes spatio-temporal correlations within this latent token space, enhancing prediction smoothness and accuracy while

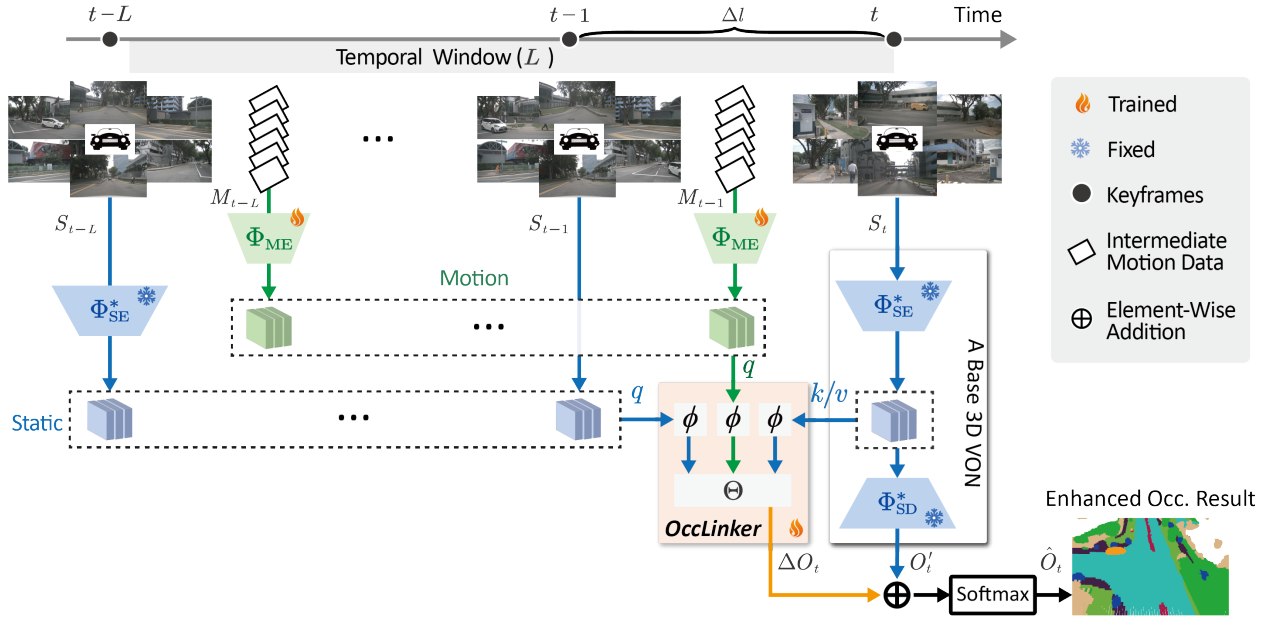


Fig. 3: Overview of OccLinker. A frozen base 3D VON [13], [17], [26] runs at a fixed frequency to extract static texture features by Φ_{SE}^* and generate initial occupancy prediction by Φ_{SD}^* . We employ Φ_{ME} for extracting motion features of intermediate frame differences, and OccLinker uses the static and motion features from the recent temporal window as queries, and the current static feature as the key and value. Through lightweight tokenization encoder ϕ and dual cross-attention module Θ , it constructs spatio-temporal correlations and outputs a correction term ΔO_t to refine the initial prediction.

compensating for missing voxels in the current occupancy estimate. The resulting enhancement component ΔO_t is formulated as:

$$\Delta O_t = \Theta(\phi(s_{t-L:t}), \phi(m_{t-L:t-1})). \quad (3)$$

Then, the final enhanced occupancy prediction becomes:

$$\hat{O}_t = \text{Softmax}(O'_t + \Delta O_t). \quad (4)$$

Here, O'_t and ΔO_t denote the occupancy logits, each with a shape of $C \times H \times W \times D$, where C is the number of semantic occupancy classes, and H , W , and D correspond to the height, width, and depth (length) of the 3D occupancy data, respectively. The $\text{Softmax}(\cdot)$ function is applied along the class dimension to convert the logits into class probabilities.

Notably, our method focuses on enhancing the current-frame occupancy using historical and motion cues, rather than forecasting future occupancy. The design principle emphasizes lightweight integration without retraining or modifying the base network. Fig. 3 presents the overall design of our OccLinker. In contrast to previous approaches [12], [14]–[18] that depend on redundant historical data, OccLinker compute the enhancement component ΔO_t using a dual cross-attention mechanism [36], designed to distill essential cues from both static and motion features while capturing compact latent correlations. First, we apply a sparse tokenization strategy to transform $s_{t-L:t}$ and $m_{t-L:t}$ into two separate sets of queries, as described in Section III-B. Then, we establish spatio-temporal correlation in a compact shared latent space, detailed in Section III-C. Finally, the optimization procedure is described in Section III-D, and the pseudo-code for the OccLinker inference pipeline is summarized in Algorithm 1.

B. Sparse tokenization for query construction

To effectively extract static and motion cues for downstream correlation modeling, we first encode the raw inputs into compact token representations. This process is composed of two parallel modules: a static feature encoder (SE) and a motion feature encoder (ME), followed by a lightweight tokenization encoder (TE).

a) Static feature encoder: We extract static spatial features from both the current and previous keyframes by directly reusing the 2D vision backbone modules, denoted as Φ_{SE} , from foundational vision-based occupancy networks (e.g., SurroundOcc [13] or ViewFormer [17]). Let S_t represent the current surround-view image and $S_{t-L:t-1}$ denotes the historical keyframes within a temporal window of size L . The corresponding static features are computed as:

$$s_{t-L:t} = \Phi_{SE}^*(S_{t-L:t}), \quad (5)$$

where Φ_{SE}^* shares parameters across all time steps.

b) Motion feature encoder: Although occupancy prediction is typically performed using keyframes sampled at a fixed rate, the ego-vehicle continuously captures high-frequency RGB images. These intermediate frames, located between consecutive keyframes, contain rich motion cues that are valuable for spatial-temporal perception. To efficiently extract motion information, we adopt a simple yet effective frame-difference technique [56]. For each pair of adjacent keyframes (S_i, S_{i+1}) within the historical window $[t-L, t]$, where $t-L \leq i < i+1 \leq t$. We compute the difference between any two intermediate frames indexed by (τ_a, τ_b) satisfying $i \leq \tau_a < \tau_b \leq i+1$:

$$F_{i:i+1} = \{S_{i:i+1}^{\tau_b} - S_{i:i+1}^{\tau_a}\}. \quad (6)$$

Algorithm 1: OccLinker inference pipeline

Input: Keyframes $S_{t-L:t}$ and motion cues $M_{t-L:t}$;
 Frozen static encoder Φ_{SE}^* and decoder Φ_{SD}^* from the base VON; Trainable motion encoder Φ_{ME} and trainable components in OccLinker, including tokenization encoder ϕ and dual cross-attention module Θ .

Output: Enhanced occupancy prediction \hat{O}_t .

- 1 Initialize temporal context window $\mathcal{W} \leftarrow \emptyset$, $|\mathcal{W}| = L$;
- 2 **while** True **do**
- // Stage 1: Base VON Inference
- Extract static features from the current frame:
 $s_t \leftarrow \Phi_{\text{SE}}^*(S_t)$;
- Predict initial occupancy logits: $O'_t \leftarrow \Phi_{\text{SD}}^*(s_t)$;
- // Stage 2: Spatio-Temporal Linking
- Extract motion features from the high-frequency motion cues: $m_t \leftarrow \Phi_{\text{ME}}(M_t)$;
- Append (s_t, m_t) to the temporal window \mathcal{W} and discard the oldest entry if $|\mathcal{W}| > L$;
- Retrieve recent static and motion features $s_{t-L:t-1}$, $m_{t-L:t-1}$, and s_t from \mathcal{W} ;
- Convert all retrieved features into sparse tokens via Eq. (9);
- Establish spatio-temporal correlations within these tokens via Eq. (10);
- Decode the attention outputs into a correction component via Eq. (11);
- // Stage 3: Occupancy Refinement
- Refine the initial occupancy prediction via Eq. (4);
- Advance to the next timestep: $t \leftarrow t + 1$;
- 13 **end**

All such differences across the L intervals are concatenated as the motion input:

$$M_{t-L:t-1} = \text{Concat}(\{F_{i:i+1} \mid i \in [t-L, t-1]\}), \quad (7)$$

where $\text{Concat}(\cdot)$ denotes the concatenation operation performed along the temporal dimension, combining motion cues from all intervals in the historical window.

The resulting difference images $M_{t-L:t}$ are then used as input to the motion encoding module. Since these frame difference images typically share the same resolution as the original RGB images – often high-resolution [57] (e.g., 1600×900) – direct processing can be expensive and unsuitable for real-time applications. To address this, we first downsample $M_{t-L:t-1}$ by a factor of five to reduce the spatial dimensions. Moreover, unlike RGB images that contain complex textures and color variations, frame difference images primarily capture motion boundaries. Therefore, we employ a lightweight three-layer convolutional neural network (CNN) followed by batch normalization (BN) to efficiently extract motion cues. This network is denoted by Φ_{ME} . Formally, the resulting motion features are computed as:

$$m_{t-L:t-1} = \Phi_{\text{ME}}(M_{t-L:t-1}). \quad (8)$$

c) Sparse tokenization encoder: The extracted feature s_t , $s_{t-L:t-1}$, and $m_{t-L:t-1}$ are then fed into a shared tokenization encoder that transforms them into compact token sets. Specifically, a 1×1 convolution is applied to first reduce channel dimensions, followed by a spatial unfolding operation that divides each image into $p \times p$ patches. Within each patch, pixel-wise features are averaged to form a v -dimensional vector. This process is applied to each camera view independently and results in the following tokenization operation ϕ :

$$\phi(I) = \overline{\mathcal{U}(p, p)(I \otimes \Theta_{1 \times 1})}, \quad (9)$$

where I is the input feature, \otimes denotes convolution, $\Theta_{1 \times 1}$ is a 1×1 kernel, and $\mathcal{U}(p, p)$ represents patch unfolding. The averaging operator $\overline{\cdot}$ produces a compact representation per spatial patch.

The final output E is a set of sparse tokens with shape $[|V| \cdot \lfloor \frac{h}{p} \rfloor \cdot \lfloor \frac{w}{p} \rfloor, 1, d_{\text{token}}]$, where each token retains localized spatial or motion semantics. This tokenized format is especially well-suited for attention-based fusion in our multi-stream integration module, as discussed next.

C. Spatio-temporal correlation strategy

To efficiently exploit historical static and motion cues while avoiding redundant computation, we adopt a spatio-temporal correlation strategy based on dual multi-head attention operations. Unlike previous approaches that directly fuse all temporal inputs indiscriminately [5], [14], our method disentangles the correlation modeling process into two independent streams: one for static context and another for motion cues. These correlations are computed in a shared compact latent space, improving both interpretability and efficiency.

a) Cross-attention-based spatio-temporal reasoning:

Given the sparse tokens s_t , $s_{t-L:t-1}$, and $m_{t-L:t-1}$ extracted in Section III-B, we use s_t (the current frame token) as the reference context. The goal is to model how past appearance and motion features relate to the current frame through dual multi-head attention mechanisms (MHAM) [36].

- **Historical static attention:** We use the tokenized historical static features $\phi(s_{t-L:t-1})$ as queries (Q_{sta}), while the tokenized current feature $\phi(s_t)$ serves as both keys (K_{cur}) and values (V_{cur}). Each component is projected into a shared latent space via independent learnable transformations. This MHAM produces the output f_{sta} , capturing long-range spatial appearance correlations, as illustrated in the first column of Fig. 4.
- **Historical motion attention:** Similarly, the motion tokens $\phi(m_{t-L:t-1})$ are used as queries (Q_{mot}), and the same current feature tokens $\phi(s_t)$ are reused as keys (K_{cur}) and values (V_{cur}). The resulting attention output f_{mot} captures temporally aligned motion dynamics, as shown in the second column of Fig. 4.

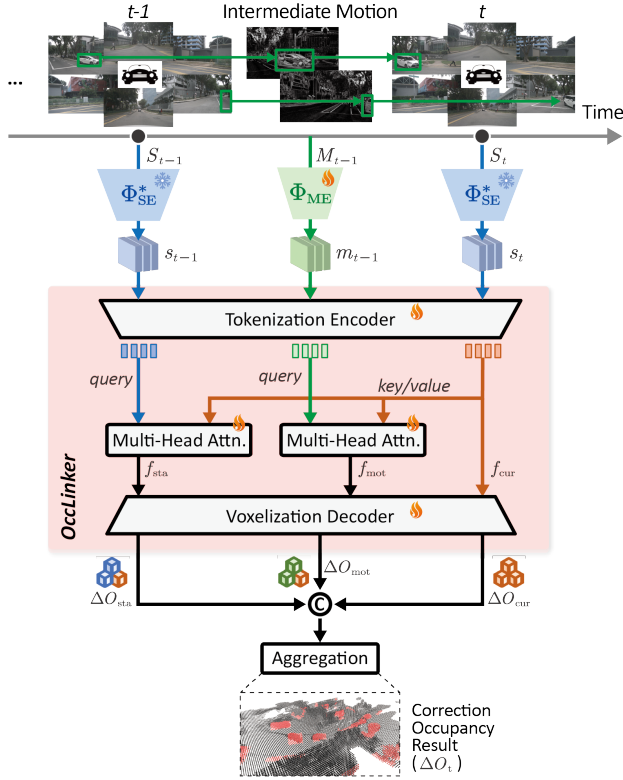


Fig. 4: Correlation pipeline in OccLinker. Using $L = 1$ as an example, OccLinker explicitly separates static and dynamic correlations by treating current static features as keys and values, while using historical static features and intermediate motion features as queries.

Each attention stream is formulated as:

$$\begin{aligned} f_{sta} &= \text{Softmax} \left(\frac{W_{sta}^Q Q_{sta} (W_{cur}^K K_{cur})^\top}{\sqrt{d_{\text{grad}}}} \right) (W_{cur}^V V_{cur}), \\ f_{mot} &= \text{Softmax} \left(\frac{W_{mot}^Q Q_{mot} (W_{cur}^K K_{cur})^\top}{\sqrt{d_{\text{grad}}}} \right) (W_{cur}^V V_{cur}), \end{aligned} \quad (10)$$

where W_*^Q , W_*^K , and W_*^V are independent learnable projection matrices for each stream. The $\text{Softmax}(\cdot)$ function is used to normalize the attention scores, and the scaling factor $\sqrt{d_{\text{grad}}}$ helps stabilize gradients during training [36].

b) *Feature decoding and correction:* The attention outputs f_{sta} and f_{mot} , together with the current token $f_{cur} = K_{cur}$, are passed through separate lightweight decoding heads to reconstruct the spatio-temporal correction signal ΔO_t . Each stream is first reshaped using 3D deconvolution layers followed by ReLU activations to recover the spatial dimensions. The decoding network is parameterized by Θ_D . This produces three correction results: ΔO_{sta} from static attention, ΔO_{mot} from motion attention, and ΔO_{cur} from the current frame as the baseline. These results are then concatenated along the feature channel and aggregated using an additional 3D convolutional layer:

$$\Delta O_t = \text{Concat}(\{\Delta O_{sta}, \Delta O_{mot}, \Delta O_{cur}\}) \otimes \Theta_{3 \times 3 \times 3}, \quad (11)$$

where $\Theta_{3 \times 3 \times 3}$ is a learnable 3D convolution kernel.

The fused correction ΔO_t is then added to the initial occupancy logits O'_t from the base model, as defined in Eq. (4), yielding the final enhanced prediction \hat{O}_t . This integration augments the base prediction with temporally aligned static and motion-aware cues, while maintaining full compatibility with any existing foundational VONs.

The proposed correlation design improves both interpretability and efficiency by explicitly separating static and dynamic contexts, enabling robust enhancement without modifying the backbone network.

Notably, we do not rely on any explicit coordinate transformation between frame t and historical frames $t - L : t - 1$. Unlike many occupancy prediction methods [10], [17] that incorporate ego-motion information (e.g., relative translation and rotation from IMU or odometry) for geometric alignment or implicit motion compensation, OccLinker directly associates historical static and dynamic cues in the sparse latent space. This design keeps OccLinker lightweight, sensor-agnostic, and fully compatible with both single-frame and history-aware VONs, without requiring additional motion supervision or modifying their original coordinate systems.

D. Optimization

As shown in Fig. 3, the static encoder Φ_{SE} is directly inherited from well-established VON architectures [13], [17], [26]. In contrast, the motion encoder Φ_{ME} is a lightweight, trainable module specifically designed to extract temporal dynamics and compensate for missing or incomplete voxel predictions caused by occlusions or visual ambiguity. In scenarios where the static encoder Φ_{SE} produces suboptimal outputs, Φ_{ME} serves as a complementary component by injecting motion-aware corrections. Notably, the motion encoder is unlikely to dominate or collapse unless the frozen static features are already sufficiently complete to support accurate occupancy predictions on their own.

To maintain stability and efficiency during training, we freeze the static encoder Φ_{SE} and only optimize the proposed enhancement module OccLinker along with the motion encoder Φ_{ME} . This design yields two key advantages: (1) it avoids potential gradient interference in Φ_{SE} , ensuring more stable optimization; and (2) it accelerates convergence of our plug-in module by leveraging reliable static features extracted by the pre-trained backbone.

To ensure a fair comparison and retain consistency with prior work, we adopt the original loss functions used by each benchmark during training. For the SurroundOcc [13] benchmark, we employ the following composite loss function:

$$\mathcal{L} = \mathcal{L}_{ce} + \mathcal{L}_{sem} + \mathcal{L}_{geo}, \quad (12)$$

where \mathcal{L}_{ce} is a voxel-wise cross-entropy loss for occupancy classification [58], \mathcal{L}_{sem} enforces semantic consistency across space [59], \mathcal{L}_{geo} encourages geometric coherence between neighboring voxels [60].

For the Occ3D [7] benchmark, following the convention in ViewFormer [17], we apply the following loss:

$$\mathcal{L} = \mathcal{L}_{focal} + \mathcal{L}_{ce} + \mathcal{L}_{ls} + \lambda \mathcal{L}_{l1}, \quad (13)$$

where $\mathcal{L}_{\text{focal}}$ is the focal loss [61] for handling class imbalance, \mathcal{L}_{ls} is the lovasz softmax loss [62] for improving boundary-level segmentation, \mathcal{L}_{l1} is an L1 regression loss (scaled by λ) to supervise motion-induced voxel correction.

IV. EXPERIMENTS

A. Experimental settings

a) *Benchmark*: We evaluate on two established occupancy benchmarks: (i) the SurroundOcc benchmark [13], [57], which generates occupancy labels by voxelizing aggregated multi-frame LiDAR in the ego frame, using manually annotated 3D bounding boxes to assign semantic categories; and (ii) the Occ3D benchmark [7], which provides 0.4m-resolution voxel-level labels with occlusion states through automated LiDAR aggregation and mesh reconstruction. Both benchmarks cover 1,050 driving scenes, each with up to 40 timestamped frames and six synchronized cameras (front, front-left/right, back, back-left/right) at 1600×900 resolution. In our experiments, we enhance single-frame baselines [13], [17], [26] by aggregating features from L historical keyframes. Additionally, unlabeled intermediate frames from the “sweeps” folder [57] are utilized as motion information for OccLinker.

b) *Implementation details*: Both the SurroundOcc and Occ3D benchmarks adopt the same 3D occupancy resolution of $(H, W, D) = (200, 200, 16)$ and utilize the same number of surround-view cameras, with $|V| = 6$. However, they differ in semantic granularity: SurroundOcc defines $C = 17$ semantic classes, while Occ3D provides $C = 18$ for finer-grained occupancy labeling. Following the respective conventions [13], [17] for static feature dimensions, we adopt a feature map resolution of $(h, w) = (116, 200)$ for SurroundOcc and $(h, w) = (32, 88)$ for Occ3D. Notably, both $s_{t-L:t}$ and $m_{t-L:t}$ share the same dimensionality of $|V| \times c \times w \times h$.

We employ the Φ_{ME} module with a temporal sampling interval of $\Delta t \approx 0.1$ seconds to extract motion features from raw nuScenes images at a resolution of 900×1600 . Within the Φ_{ME} module, input images are first downsampled by a factor of 5, resulting in 180×320 feature maps to reduce GPU memory consumption. Motion inputs are computed using either frame difference operations [56] or optical flow analysis [63]. The token dimension and the gradient scaling factor are both set to $d_{\text{token}} = d_{\text{grad}} = 32$, with the number of temporal patches set as $p = 6$. For the convolutional layer $\Theta_{1 \times 1}$, the kernel size, stride, padding, input channels, and output channels are set to $(1, 1)$, 1, 0, 512, and d_{token} , respectively. In contrast, for $\Theta_{3 \times 3 \times 3}$, these values are set to $(3, 3, 3)$, 1, 1, $3C$, and C , respectively. OccLinker is integrated on top of this baseline to complement the missing inter-frame motion cues, rather than replacing any component of the original design.

All experiments were conducted using four NVIDIA L20 GPUs with a batch size of 1. We employed the AdamW optimizer on both the SurroundOcc [13] and Occ3D [7] benchmarks, setting the learning rate to 2×10^{-4} , weight decay to 1×10^{-2} , and betas to $(0.9, 0.999)$. The overall training took approximately 24 epochs, corresponding to about 1.5 GPU-days in total, including around 1.4 GPU-days for pretraining the base VON and 0.1 GPU-day for fine-tuning OccLinker.

B. Evaluation Metrics

a) *Occupancy accuracy metric*: For a rigorous and comprehensive evaluation across benchmarks, we employ Intersection over Union (IoU) and Mean Intersection over Union (mIoU) metrics, which are standard in 3D semantic occupancy prediction tasks [64]–[67]. IoU measures the global overlap between all predicted occupied voxels and their ground-truth counterparts, regardless of semantic categories. It reflects the overall spatial accuracy of the 3D occupancy prediction. In contrast, mIoU is the mean IoU computed by averaging IoUs over all semantic classes, which reflects class-balanced semantic accuracy.

To further evaluate the temporal consistency and occupancy accuracy for both moving and static objects, we adopt the object categorization scheme from Cam4DOcc [54], dividing objects into two broad classes: General Moving Objects (GMO) and General Static Objects (GSO). Objects that remain stationary relative to the ground are classified as GSO, whereas those that move relative to the ground belong to the GMO category. This classification scheme enables a fine-grained and quantitative analysis of moving and static objects within the scene. Detailed semantic categories for each class are listed in Table I. The mIoU scores are reported separately for three groups: all classes, GMO classes, and GSO classes.

Classification	GMO	GSO
Semantic category	bicycle, bus, car, construction_vehicle, motorcycle, pedestrian, trailer, truck	others, noise, traffic_cone, driveable_surface, other_flat, sidewalk, terrain, manmade, vegetation

Table I: Details of semantic classification. Compared to SurroundOcc, Occ3D includes an additional “others” category under GSO. Both benchmarks also contain an “unoccupied” category, which does not belong to either GMO or GSO.

b) *Temporal consistency metric*: To quantify the temporal stability gained by integrating OccLinker with baseline models, we introduce a temporal consistency metric designed to detect and measure changes between consecutive frames. This metric reflects the smoothness and stability of predictions, which is crucial for enhancing the user’s visual experience.

Let $\sigma_{i,n}^{(x,y,z)}$ denote the semantic label of the n -th voxel at spatial coordinates (x, y, z) in frame i . Define the indicator function $\delta(e_1, e_2) = \mathbb{I}(e_1 \neq e_2)$, which equals 1 if the two inputs differ and 0 otherwise. Voxel changes between frames i and j fall into two categories: “Moving Object Change” (MOC) and “Static Object Change” (SOC), defined as follows:

Type	Condition
MOC	$\sigma_{i,n}^{(x,y,z)} \in \text{GMO}$ or $\sigma_{j,n}^{(x,y,z)} \in \text{GMO}$
SOC	$\sigma_{i,n}^{(x,y,z)} \in \text{GSO}$ and $\sigma_{j,n}^{(x,y,z)} \in \text{GSO}$

Table II: Definitions of MOC and SOC voxel changes.

Using these definitions, we define disparity metrics Δ_m and Δ_s to quantify temporal inconsistencies between frames i and

j , as follows:

$$\begin{aligned}\Delta_m(i, j) &= \frac{1}{N_{mc}} \sum_{n=1}^{N_{mc}} \delta \left(\sigma_{i,n}^{(x,y,z)}, \sigma_{j,n}^{(x,y,z)} \right), \\ \Delta_s(i, j) &= \frac{1}{N_{sc}} \sum_{n=1}^{N_{sc}} \delta \left(\sigma_{i,n}^{(x,y,z)}, \sigma_{j,n}^{(x,y,z)} \right).\end{aligned}\quad (14)$$

where N_{mc} and N_{sc} represent the number of corresponding voxels in the moving and static regions, respectively.

The overall temporal consistency scores for moving and static objects, S_m and S_s , are then computed by aggregating disparities over sequential frames:

$$S_{m/s} = 1 - \frac{1}{M-1} \sum_{k=1}^{M-1} \Delta_{m/s}(k, k+1), \quad (15)$$

where M denotes the total number of frames in the scene. Final consistency scores \overline{S}_m and \overline{S}_s are averaged across all scenes. Higher values indicate smoother and more temporally consistent occupancy predictions.

C. Comparison Results

a) Occupancy accuracy on SurroundOcc benchmark:

We compare our method with several state-of-the-art models, including single-frame VON methods such as Atlas [68], TPVFormer [47], MonoScene [26], and SurroundOcc [13], as well as history-aware VON methods such as BEVFormer [69] and BEVDet4D-Occ [14]. To ensure a fair comparison, all baselines and OccLinker are trained on the same ground truth data using identical training protocols. As shown in Table III, integrating OccLinker into existing baselines like MonoScene [26] and SurroundOcc [13] leads to notable performance gains. In particular, the combination of OccLinker with SurroundOcc achieves the best results among all models, improving IoU and mIoU (All) by 1.63% and 0.37%, respectively. Moreover, compared with BEVFormer, which incorporates historical BEV features, our method further boosts performance by 0.41% in IoU and 0.34% in mIoU.

b) Occupancy accuracy on Occ3D benchmark:

We also evaluate our method on the Occ3D benchmark [7], as shown in Table IV. The baselines include single-frame VON methods such as MonoScene [26], OccFormer [1], SurroundOcc [13], and ViewFormer [17], as well as history-aware VON methods including SparseOcc [16], BEVDet4D-Occ [14], and OPUS-L [15]. When integrated into single-frame VONs, OccLinker consistently improves the performance of the base models. Furthermore, in ViewFormer+OccLinker, ViewFormer maintains a memory queue in which each frame's intermediate BEV feature interacts with historical multi-frame BEV representations, while our method further supplements the missing sparse motion features between frames. As a result, ViewFormer+OccLinker surpasses ViewFormer by 0.24% in IoU and 0.94% in mIoU (All).

We note that in Table IV, ViewFormer achieves higher IoU than SurroundOcc, while this advantage is not reflected in \overline{S}_s . This is mainly because ViewFormer attains higher IoU by aggregating multi-frame BEV features, which captures richer geometric context for individual frames. However, its complex

Method	IoU \uparrow	mIoU \uparrow			$\overline{S}_m \uparrow$	$\overline{S}_s \uparrow$
		All	GMO	GSO		
Single-frame VON methods						
Atlas [68]	28.66	15.00	12.64	17.35	—	—
TPVFormer [47]	30.86	17.10	14.04	20.15	—	—
MonoScene [26]	10.04	1.15	0.24	2.07	46.53	81.77
+OccLinker	13.10	1.69	0.34	3.04	54.21	83.84
Δ	+3.06	+0.54	+0.10	+0.97	+7.68	+2.07
SurroundOcc [13]	31.49	20.30	18.39	22.20	58.33	91.71
+OccLinker	33.12	20.67	18.26	23.08	60.64	92.54
Δ	+1.63	+0.37	-0.13	+0.88	+2.31	+0.83
History-aware VON methods						
BEVDet4D-Occ [14]	24.26	14.22	11.10	17.34	—	—
BEVFormer [69]	30.50	16.75	14.17	19.33	52.84	84.21
+OccLinker	30.91	17.09	14.16	20.01	55.21	85.99
Δ	+0.41	+0.34	-0.01	+0.68	+2.37	+1.78

Table III: Occupancy prediction performance on the SurroundOcc benchmark [13]. Performance gains (Δ) are highlighted in **bold**, and the best results are marked with **■**.

Method	IoU \uparrow	mIoU \uparrow			$\overline{S}_m \uparrow$	$\overline{S}_s \uparrow$
		All	GMO	GSO		
Single-frame VON methods						
MonoScene [26]	—	6.06	5.36	6.68	—	—
OccFormer [1]	—	21.93	21.78	22.06	—	—
SurroundOcc [13]	51.89	7.24	0.36	13.35	65.35	89.54
+OccLinker	52.13	10.33	1.98	17.76	69.60	90.91
Δ	+0.24	+3.09	+1.62	+4.41	+4.25	+1.37
History-aware VON methods						
SparseOcc [16]	—	30.10	—	—	—	—
BEVDet4D-Occ [14]	—	39.30	29.09	42.16	—	—
OPUS-L [15]	—	36.20	31.25	40.44	—	—
ViewFormer [17]	70.39	40.46	33.73	46.45	67.26	86.06
+OccLinker	70.63	41.30	34.33	47.50	70.13	87.10
Δ	+0.24	+0.84	+0.60	+1.05	+2.87	+1.04

Table IV: Occupancy prediction performance on the Occ3D benchmark [13]. Performance gains (Δ) are highlighted in **bold**, and the best results are marked with **■**.

temporal fusion may occasionally propagate redundant or noisy historical information, resulting in less stable transitions between consecutive frames. In contrast, SurroundOcc performs frame-by-frame prediction with limited reliance on long-term history, which naturally leads to smoother temporal behavior and thus higher temporal consistency scores, albeit at the cost of lower per-frame spatial accuracy. Notably, our method improves the temporal consistency of both categories of models by explicitly enhancing sparse inter-frame correlations without introducing additional temporal noise.

c) *Temporal consistency*: The \overline{S}_m and \overline{S}_s results presented in Tables III and IV show that integrating OccLinker consistently improves the temporal consistency of occupancy predictions across all frames and scenes for all models, highlighting the effectiveness of our approach. This improvement can be attributed to the use of previous static features and the incorporation of motion information, which together provide valuable correlations between static/dynamic cues and occupancy refinement.

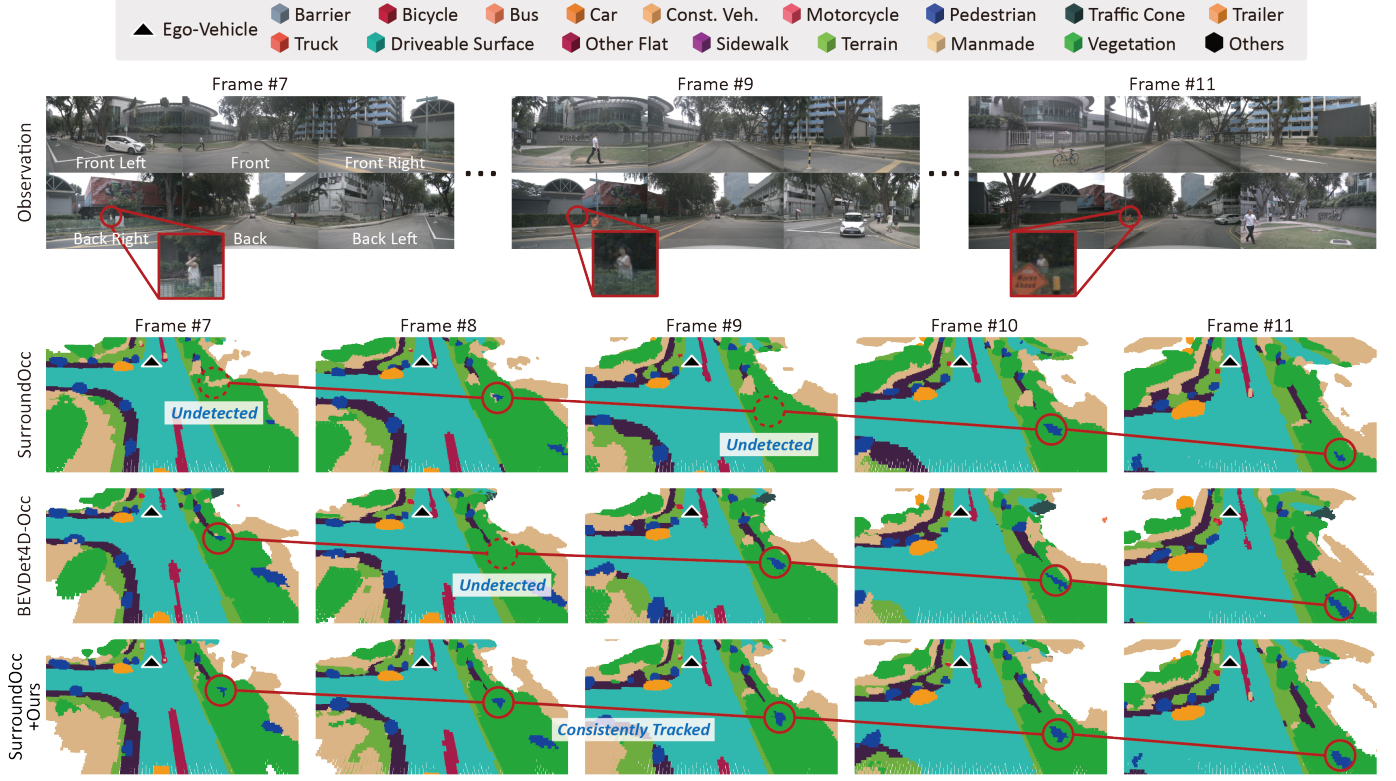


Fig. 5: Comparison in a T-junction scenario with partial and dynamic pedestrian occlusions. SurroundOcc+OccLinker produces robust predictions, with the pedestrian being consistently tracked, while SOTA methods show a flickering phenomenon.

D. Ablation study

a) *Different combinations of OccLinker:* Table V presents the ablation results of different decomposed correlation designs in OccLinker, as illustrated in Fig. 4, when integrated with SurroundOcc [13] under $L = 1$. **M0** denotes the baseline model without OccLinker. **M1** removes the correlation between historical and current static features. **M2** omits the current static features entirely. **M3** excludes the correlation between motion features and current static features. **M4[†]** reverses the roles of queries and key/value pairs in the correlation design of Fig. 4. **M4** represents the complete version of OccLinker with all components included.

The results in Table V clearly demonstrate that removing any individual stream from the OccLinker module leads to performance degradation in both prediction accuracy and temporal consistency, confirming the necessity of the decomposed correlation modeling. Moreover, the comparison between **M4[†]** and **M4** highlights that treating previous keyframes and motion features as queries – rather than as keys/values—effectively captures temporally aligned cues essential for robust occupancy refinement.

b) *Impact of different types of motion information:*

Table VI investigates the impact of different types of motion information on SurroundOcc+OccLinker when $L = 1$. Specifically, **I0** denotes the base model [13] without any motion input. **I1** uses raw high-frequency intermediate frames as motion input for OccLinker. **I2** incorporates optical flow [63], while **I3** employs frame difference [56] to extract motion cues.

As shown in Table VI, **I1** improves IoU over **I0**, but

Idx.	ΔO_{sta}	ΔO_{cur}	ΔO_{mot}	IoU \uparrow	mIoU \uparrow	$\overline{S_m} \uparrow$	$\overline{S_s} \uparrow$	
M0	x	x	x	31.49	20.30	58.33	91.71	
M1	x	✓	✓	33.04	20.04	60.59	92.25	
M2	✓	x	✓	33.05	19.98	60.09	92.44	
M3	✓	✓	x	32.88	20.10	60.24	92.24	
M4[†]	✓	✓	✓	31.97	20.11	60.19	92.01	
M4	✓	✓	✓	33.12	20.67	60.64	92.54	
					+1.63	+0.37	+2.31	+0.83

Table V: Ablation study of decomposed latent correlation modeling in OccLinker when integrated with SurroundOcc. Compared to **M4**, **M4[†]** reverses the roles of queries and key/value pairs. Performance gains over **M0** are **bolded**, and the best results are marked with **■**.

Idx.	Motion type	IoU \uparrow	mIoU \uparrow	$\overline{S_m} \uparrow$	$\overline{S_s} \uparrow$	Time \downarrow
I0	-	31.49	20.30	58.33	91.71	N/A
I1	Raw Image	32.39	19.45	59.01	91.15	N/A
I2	Optical Flow	32.80	20.27	60.53	92.13	9.221 ms
I3	Frame Diff.	33.12	20.67	60.64	92.54	6.181 ms

Table VI: Ablation study of different motion information types used in OccLinker. The best results are marked with **■**.

performs worst in mIoU, $\overline{S_m}$, and $\overline{S_s}$ among the motion-aware variants. This performance drop is largely due to the presence of redundant and irrelevant information in raw intermediate frames, which complicates the extraction of motion features by OccLinker. Moreover, **I3** significantly outperforms **I2** in both IoU and mIoU, and achieves slightly better results in $\overline{S_m}$

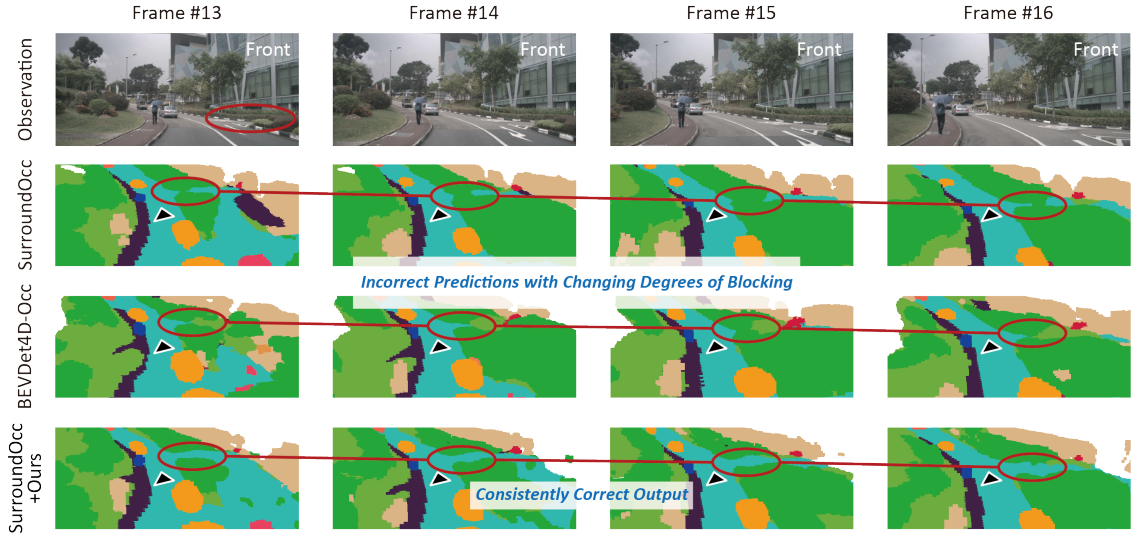


Fig. 6: Comparison in a ramp entry scenario with partial occlusions from roadside vegetation. SurroundOcc+OccLinker produces robust and continuous predictions of the drivable surface, while SOTA methods occasionally misclassify the ramp as blocked.

and $\overline{S_s}$. This suggests that frame difference is more effective at capturing abrupt scene changes, such as pedestrians suddenly appearing or vehicles exiting intersections, whereas optical flow may introduce delays in responding to such dynamics. In addition, thanks to the lightweight design of OccLinker, using frame difference further reduces computational overhead by operating on simple differential signals, thereby enhancing inference efficiency.

c) *Impact of different numbers of previous keyframes*: We conduct ablation experiments on the temporal context window length $L \in \{0, 1, 2, 3, 4\}$ in \mathcal{W} . The case of $L = 0$ corresponds to SurroundOcc [13], which does not utilize any historical keyframes. As shown in Table VII, the best IoU and mIoU are achieved when $L = 1$, while the highest $\overline{S_m}$ and $\overline{S_s}$ scores occur at $L = 2$.

Idx.	Window length L	IoU \uparrow	mIoU \uparrow	$\overline{S_m} \uparrow$	$\overline{S_s} \uparrow$
L0	0	31.49	20.30	58.33	91.71
L1	1	33.12	20.69	60.64	92.54
L2	2	31.89	20.32	61.00	92.71
L3	3	31.67	20.01	59.01	91.77
L4	4	CUDA Out of Memory			

Table VII: Effect of different number of previous keyframes. The best results are marked with ■.

When introducing historical keyframes (from $L = 0$ to $L = 1$), both occupancy accuracy metrics (IoU and mIoU) and temporal consistency metrics ($\overline{S_m}$ and $\overline{S_s}$) are improved, indicating that OccLinker enables SurroundOcc to leverage additional historical information and thus enrich temporal context. However, when L is further increased to 2, although temporal consistency continues to improve, larger values of L also introduce more irrelevant or noisy features. This makes it more challenging to associate historical information with the current occupancy prediction and may potentially lead to semantic misalignment.

Moreover, since OccLinker is designed for efficiency, in-

creasing L linearly expands the input volume and computational cost, leading to greater resource consumption during training and inference. Based on these findings, we recommend setting L to 1 or 2 as a balanced choice between performance and efficiency.

d) *Impact of different aggregation strategies in OccLinker*: As illustrated in Fig. 4, OccLinker adopts a late aggregation strategy (**S2** in Table VIII), where the learned tokens after MHAM are first passed through separate decoders and then aggregated in the occupancy space. In contrast, strategy **S1** employs early aggregation by combining the learned tokens in token space before decoding.

The results in Table VIII show that the 3D-space fusion used in **S2** yields superior performance. This is because the output of OccLinker functions more effectively as an occupancy correction term when added directly in the occupancy space. Furthermore, the additive nature of **S2**'s design aligns more naturally with the plug-and-play paradigm than the early fusion approach used in **S1**.

Idx.	Strategy	mIoU \uparrow	Memory (Test) \downarrow	Latency \downarrow
S1	Early aggregation	40.58	4,780 MB	0.1598 s
S2	Late aggregation	41.30	4,687 MB	0.1210 s

Table VIII: Effect of different aggregation strategies in ViewFormer+OccLinker. The best results are marked with ■.

E. Case analysis

To qualitatively assess the effectiveness of our method, we compare SurroundOcc+OccLinker with the a single-frame 3D VON baseline (SurroundOcc [13]) and a history-aware VON method (BEVDet4D-Occ [14]).

a) *Temporal visualization cases*: As shown in Fig. 5 (Scene 277, Frames #7–#11), a pedestrian walking along the sidewalk – parallel to the ego vehicle’s trajectory – is intermittently occluded by roadside vegetation. SurroundOcc [13]

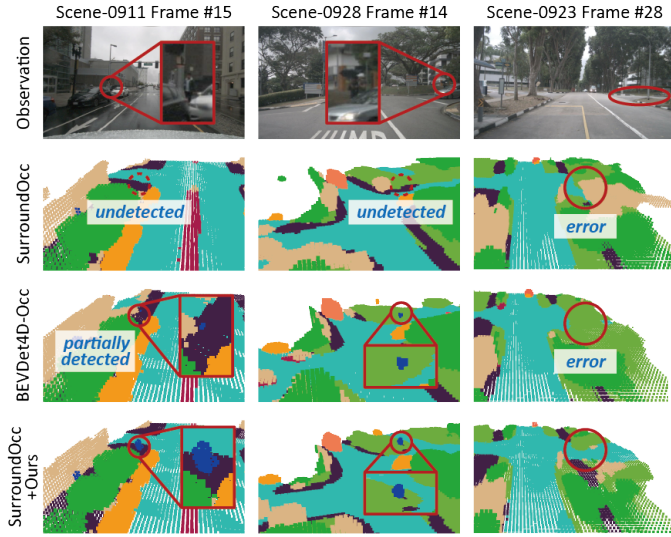


Fig. 7: Several challenging scenarios are presented: pedestrians are partially occluded by vehicles in the first and second columns, and road boundaries appear visually ambiguous in the third column. SurroundOcc+OccLinker yields more accurate predictions, while SOTA methods display noticeable artifacts.

exhibits significant instability, with the pedestrian missing in Frames #7 and #9, highlighting its limitations in temporal modeling. BEVDet4D-Occ [14] partially alleviates this issue by fusing historical latent features into the current latent space, but still shows occasional inconsistencies, such as a detection dropout in Frame #8. In contrast, SurroundOcc+OccLinker completely eliminates these flickering artifacts and achieves consistent detection across all occlusion states.

As shown in Fig. 6 (Scene 926, Frames #13-#16), in the ramp entry scenario, the front-right ramp lane in the camera front view is partially occluded by roadside vegetation. SurroundOcc+OccLinker produces robust and continuous predictions of the drivable surface at the junction, while the baseline methods exhibit flickering predictions, occasionally misclassifying the entrance as blocked.

b) Single-frame visualization cases: Fig. 7 showcases several challenging scenarios: (i) Vehicle-pedestrian occlusion (Scene-0911 Frame #15, Scene-0928 Frame #14): Both SurroundOcc [13] and BEVDet4D-Occ [14] fail to recover the occupancy state of the partially occluded pedestrian, whereas our method accurately localizes the target with precise geometry. (ii) Ambiguous road boundary (Scene-0923 Frame #28): Baseline methods produce fragmented or erroneous occupancy predictions. In contrast, our approach correctly anticipates the right-turn road geometry and preserves superior shape consistency with the actual road layout.

F. Efficiency–performance tradeoff analysis

To ensure a fair comparison, all overhead analysis experiments are conducted on a single NVIDIA L20 GPU. Table Table IX summarizes the results of several state-of-the-art methods, including history-aware approaches (FB-Occ [18],

SparseOcc [16], OPUS-L/M/S/T [15], and BEVDet4D-Occ [14]), the single-frame 3D VON baseline (ViewFormer [17]), and our method combined with ViewFormer. All models are evaluated on the Occ3D benchmark [7] using the same 2D visual encoder backbone, ResNet-50, which outputs feature maps with a resolution of (32, 88). The table reports the mIoU, GPU memory usage during inference, and per-sample latency of each method.

Model	mIoU \uparrow	Memory (Test) \downarrow	Latency \downarrow
FB-Occ [18]	39.11	5,933 MB	0.09 s
SparseOcc [16]	30.10	7,147 MB	0.05 s
OPUS-L [15]	36.20	10,579 MB	0.16 s
OPUS-M [15]	35.60	8,912 MB	0.11 s
OPUS-S [15]	34.20	7,320 MB	0.07 s
OPUS-T [15]	33.20	6,711 MB	0.03 s
BEVDet4D-Occ [14]	39.30	4,689 MB	0.26 s
ViewFormer [17]	40.46	4,582 MB	0.11 s
+OccLinker	41.30	4,687 MB	0.12 s
Δ	+0.84	+105 MB	+0.01 s

Table IX: Comparison of computational overhead. All models share the same visual encoder (Φ_{SE}) of ResNet-50 backbones. Our result (ViewFormer+OccLinker) in this table is measured for $L = 1$. OOM indicates CUDA out of memory. Performance changes (Δ) are highlighted in **bold**, and best results are marked with **■**.

The results show that ViewFormer+OccLinker achieves state-of-the-art mIoU while maintaining minimal GPU memory usage. The OccLinker plug-in consumes only 105MB, accounting for just 2.29% of ViewFormer’s memory footprint, and introduces a mere 0.01 seconds increase in inference latency. These findings confirm that OccLinker delivers competitive performance with negligible computational overhead.

V. CONCLUSION

This paper proposes OccLinker, a lightweight, plug-and-play module that seamlessly integrates with 3D VONs. OccLinker effectively extracts fine-grained discriminative features by attentively associating historical and motion features with the current feature space through decomposed cross-attention mechanisms. We introduce a new temporal consistency metric to better analyze the effectiveness of OccLinker when combined with SOTA methods in long-term predictions. Extensive visualizations validate the noticeable deflickering effect in several challenging scenarios. Future work will explore the integration of explicit instance-level supervision in occupancy tracking.

ACKNOWLEDGMENTS

The study was supported in part by Shenzhen Science and Technology Program under grant number JCYJ20241202130025030.

REFERENCES

- [1] Y. Zhang, Z. Zhu, and D. Du, “Occformer: Dual-path transformer for vision-based 3d semantic occupancy prediction,” in *Proceedings of the IEEE/CVF International Conference on Computer Vision (ICCV)*, October 2023, pp. 9433–9443.

[2] C. Zhang, J. Yan, Y. Wei, J. Li, L. Liu, Y. Tang, Y. Duan, and J. Lu, "Octnerf: Advancing 3d occupancy prediction in lidar-free environments," *IEEE Transactions on Image Processing*, vol. 34, pp. 3096–3107, 2025.

[3] Y. Li, Z. Yu, C. Choy, C. Xiao, J. M. Alvarez, S. Fidler, C. Feng, and A. Anandkumar, "Voxformer: Sparse voxel transformer for camera-based 3d semantic scene completion," in *Proceedings of the IEEE/CVF Conference on Computer Vision and Pattern Recognition (CVPR)*, June 2023, pp. 9087–9098.

[4] J. Mei, Y. Yang, M. Wang, J. Zhu, J. Ra, Y. Ma, L. Li, and Y. Liu, "Camera-based 3d semantic scene completion with sparse guidance network," *IEEE Transactions on Image Processing*, vol. 33, pp. 5468–5481, 2024.

[5] T. Yang, Y. Qian, W. Yan, C. Wang, and M. Yang, "Adaptiveocc: Adaptive octree-based network for multi-camera 3d semantic occupancy prediction in autonomous driving," *IEEE Transactions on Circuits and Systems for Video Technology*, vol. 35, no. 3, pp. 2173–2187, 2025.

[6] H. Jiang, T. Cheng, N. Gao, H. Zhang, T. Lin, W. Liu, and X. Wang, "Symphonize 3d semantic scene completion with contextual instance queries," in *Proceedings of the IEEE/CVF Conference on Computer Vision and Pattern Recognition*, 2024, pp. 20258–20267.

[7] X. Tian, T. Jiang, L. Yun, Y. Mao, H. Yang, Y. Wang, Y. Wang, and H. Zhao, "Occ3d: A large-scale 3d occupancy prediction benchmark for autonomous driving," in *Advances in Neural Information Processing Systems*, vol. 36, 2023, pp. 64318–64330.

[8] R. Liu, W. Wang, and Y. Yang, "Volumetric environment representation for vision-language navigation," in *Proceedings of the IEEE/CVF Conference on Computer Vision and Pattern Recognition*, 2024, pp. 16317–16328.

[9] H. Li, Z. Li, N. Ü. Akmandor, H. Jiang, Y. Wang, and T. Padır, "Stereovoxelnet: Real-time obstacle detection based on occupancy voxels from a stereo camera using deep neural networks," in *2023 IEEE International Conference on Robotics and Automation (ICRA)*. IEEE, 2023, pp. 4826–4833.

[10] H. Xu, P. Peng, X. Zhang, G. Tan, Y. Li, S. Wang, and L. Li, "Exploiting continuous motion clues for vision-based occupancy prediction," in *Proceedings of the AAAI Conference on Artificial Intelligence*, vol. 39, no. 8, 2025, pp. 8860–8868.

[11] H. Xu, P. Peng, G. Tan, Y. Chang, Y. Zhao, and Y. Tian, "Temporal triplane transformers as occupancy world models," *arXiv preprint arXiv:2503.07338*, 2025.

[12] W. Ouyang, Z. Xu, B. Shen, J. Wang, and Y. Xu, "Linkocc: 3d semantic occupancy prediction with temporal association," *IEEE Transactions on Circuits and Systems for Video Technology*, vol. 35, no. 2, pp. 1374–1384, 2025.

[13] Y. Wei, L. Zhao, W. Zheng, Z. Zhu, J. Zhou, and J. Lu, "Surroundocc: Multi-camera 3d occupancy prediction for autonomous driving," in *Proceedings of the IEEE/CVF International Conference on Computer Vision (ICCV)*, October 2023, pp. 21729–21740.

[14] J. Huang and G. Huang, "Bevdet4d: Exploit temporal cues in multi-camera 3d object detection," *arXiv preprint arXiv:2203.17054*, 2022.

[15] J. Wang, Z. Liu, Q. Meng, L. Yan, K. Wang, J. Yang, W. Liu, Q. Hou, and M.-M. Cheng, "Opus: occupancy prediction using a sparse set," *arXiv preprint arXiv:2409.09350*, 2024.

[16] H. Liu, H. Wang, Y. Chen, Z. Yang, J. Zeng, L. Chen, and L. Wang, "Fully sparse 3d panoptic occupancy prediction," *arXiv preprint arXiv:2312.17118*, 2023.

[17] J. Li, X. He, C. Zhou, X. Cheng, Y. Wen, and D. Zhang, "Viewformer: Exploring spatiotemporal modeling for multi-view 3d occupancy perception via view-guided transformers," in *European Conference on Computer Vision*. Springer, 2024, pp. 90–106.

[18] Z. Li, Z. Yu, D. Austin, M. Fang, S. Lan, J. Kautz, and J. M. Alvarez, "Fb-occ: 3d occupancy prediction based on forward-backward view transformation," *arXiv preprint arXiv:2307.01492*, 2023.

[19] Y. Wang, Y. Chen, X. Liao, L. Fan, and Z. Zhang, "Panoocc: Unified occupancy representation for camera-based 3d panoptic segmentation," in *Proceedings of the IEEE/CVF conference on computer vision and pattern recognition*, 2024, pp. 17158–17168.

[20] D. Chen, H. Zheng, J. Fang, X. Dong, X. Li, W. Liao, T. He, P. Peng, and J. Shen, "Rethinking temporal fusion with a unified gradient descent view for 3d semantic occupancy prediction," in *Proceedings of the Computer Vision and Pattern Recognition Conference*, 2025, pp. 1505–1515.

[21] C. Min, D. Zhao, L. Xiao, J. Zhao, X. Xu, Z. Zhu, L. Jin, J. Li, Y. Guo, J. Xing, L. Jing, Y. Nie, and B. Dai, "Driveworld: 4d pre-trained scene understanding via world models for autonomous driving," in *Proceedings of the IEEE/CVF Conference on Computer Vision and Pattern Recognition (CVPR)*, June 2024, pp. 15522–15533.

[22] Z. Ye, T. Jiang, C. Xu, Y. Li, and H. Zhao, "Cvt-occ: Cost volume temporal fusion for 3d occupancy prediction," in *European Conference on Computer Vision*. Springer, 2024, pp. 381–397.

[23] G. Oh, S. Kim, H. Ko, H.-g. Chi, J. Kim, D. Lee, D. Ji, S. Choi, S. Jang, and S. Kim, "3d occupancy prediction with low-resolution queries via prototype-aware view transformation," in *Proceedings of the Computer Vision and Pattern Recognition Conference*, 2025, pp. 17134–17144.

[24] Z. Liao, P. Wei, S. Chen, H. Wang, and Z. Ren, "Stocco: Sparse spatial-temporal cascade renovation for 3d occupancy and scene flow prediction," in *Proceedings of the Computer Vision and Pattern Recognition Conference*, 2025, pp. 1516–1526.

[25] H. Jiang, L. Liu, T. Cheng, X. Wang, T. Lin, Z. Su, W. Liu, and X. Wang, "Gausstr: Foundation model-aligned gaussian transformer for self-supervised 3d spatial understanding," in *Proceedings of the Computer Vision and Pattern Recognition Conference*, 2025, pp. 11960–11970.

[26] A.-Q. Cao and R. de Charette, "Monoscene: Monocular 3d semantic scene completion," in *Proceedings of the IEEE/CVF Conference on Computer Vision and Pattern Recognition (CVPR)*, June 2022, pp. 3991–4001.

[27] M. Wilczkowiak, E. Boyer, and P. Sturm, "Camera calibration and 3d reconstruction from single images using parallelepipeds," in *Proceedings Eighth IEEE International Conference on Computer Vision. ICCV 2001*, vol. 1, 2001, pp. 142–148 vol.1.

[28] M. Polic, W. Forstner, and T. Pajdla, "Fast and accurate camera covariance computation for large 3d reconstruction," in *Proceedings of the European Conference on Computer Vision (ECCV)*, September 2018.

[29] S. E. Hazzat, M. Merras, N. E. Akkad, A. Saaidi, and K. Satori, "3d reconstruction system based on incremental structure from motion using a camera with varying parameters," *The Visual Computer*, vol. 34, no. 10, pp. 1443–1460, 2018.

[30] Q. Fu, Q. Xu, Y. S. Ong, and W. Tao, "Geo-neus: Geometry-consistent neural implicit surfaces learning for multi-view reconstruction," in *Advances in Neural Information Processing Systems*, S. Koyejo, S. Mohamed, A. Agarwal, D. Belgrave, K. Cho, and A. Oh, Eds., vol. 35. Curran Associates, Inc., 2022, pp. 3403–3416.

[31] M. Oechsle, S. Peng, and A. Geiger, "Unisurf: Unifying neural implicit surfaces and radiance fields for multi-view reconstruction," in *Proceedings of the IEEE/CVF International Conference on Computer Vision (ICCV)*, October 2021, pp. 5589–5599.

[32] Y. Shi, T. Cheng, Q. Zhang, W. Liu, and X. Wang, "Occupancy as set of points," in *European Conference on Computer Vision*. Springer, 2024, pp. 72–87.

[33] D. Azinović, R. Martin-Brualla, D. B. Goldman, M. Nießner, and J. Thies, "Neural rgb-d surface reconstruction," in *Proceedings of the IEEE/CVF Conference on Computer Vision and Pattern Recognition (CVPR)*, June 2022, pp. 6290–6301.

[34] H. Pan, T. Guan, Y. Luo, L. Duan, Y. Tian, L. Yi, Y. Zhao, and J. Yu, "Dense 3d reconstruction combining depth and rgb information," *Neurocomputing*, vol. 175, pp. 644–651, 2016.

[35] H. Ni, J. Sun, L. Ma, D. Liu, H. Zhang, and S. Zhou, "Research on 3d image reconstruction of sparse power lines by array gm-apd lidar," *Optics & Laser Technology*, vol. 168, p. 109987, 2024.

[36] A. Vaswani, "Attention is all you need," *Advances in Neural Information Processing Systems*, 2017.

[37] Z. Zhou, Y. Zhang, and H. Foroosh, "Panoptic-polarnet: Proposal-free lidar point cloud panoptic segmentation," in *Proceedings of the IEEE/CVF Conference on Computer Vision and Pattern Recognition (CVPR)*, June 2021, pp. 13194–13203.

[38] S. Zuo, W. Zheng, Y. Huang, J. Zhou, and J. Lu, "Pointocc: Cylindrical tri-perspective view for point-based 3d semantic occupancy prediction," 2023.

[39] H. Li, Y. Hou, X. Xing, Y. Ma, X. Sun, and Y. Zhang, "Occmamba: Semantic occupancy prediction with state space models," in *Proceedings of the Computer Vision and Pattern Recognition Conference*, 2025, pp. 11949–11959.

[40] R. Cheng, C. Agia, Y. Ren, X. Li, and L. Bingbing, "S3cnet: A sparse semantic scene completion network for lidar point clouds," in *Proceedings of the 2020 Conference on Robot Learning*, ser. Proceedings of Machine Learning Research, J. Kober, F. Ramos, and C. Tomlin, Eds., vol. 155. PMLR, 16–18 Nov 2021, pp. 2148–2161.

[41] J. Li, Y. Liu, D. Gong, Q. Shi, X. Yuan, C. Zhao, and I. Reid, "Rgbd based dimensional decomposition residual network for 3d semantic scene completion," in *Proceedings of the IEEE/CVF Conference on Computer Vision and Pattern Recognition (CVPR)*, June 2019.

[42] J. Li, K. Han, P. Wang, Y. Liu, and X. Yuan, "Anisotropic convolutional networks for 3d semantic scene completion," in *Proceedings of the*

IEEE/CVF Conference on Computer Vision and Pattern Recognition (CVPR), June 2020.

[43] S. Liu, Y. HU, Y. Zeng, Q. Tang, B. Jin, Y. Han, and X. Li, “See and think: Disentangling semantic scene completion,” in *Advances in Neural Information Processing Systems*, S. Bengio, H. Wallach, H. Larochelle, K. Grauman, N. Cesa-Bianchi, and R. Garnett, Eds., vol. 31. Curran Associates, Inc., 2018.

[44] S. Li, C. Zou, Y. Li, X. Zhao, and Y. Gao, “Attention-based multi-modal fusion network for semantic scene completion,” *Proceedings of the AAAI Conference on Artificial Intelligence*, vol. 34, no. 07, pp. 11402–11409, Apr. 2020.

[45] J. Li, Y. Liu, X. Yuan, C. Zhao, R. Siegwart, I. Reid, and C. Cadena, “Depth based semantic scene completion with position importance aware loss,” *IEEE Robotics and Automation Letters*, vol. 5, no. 1, pp. 219–226, 2020.

[46] M. Garbade, Y.-T. Chen, J. Sawatzky, and J. Gall, “Two stream 3d semantic scene completion,” in *Proceedings of the IEEE/CVF Conference on Computer Vision and Pattern Recognition (CVPR) Workshops*, June 2019.

[47] Y. Huang, W. Zheng, Y. Zhang, J. Zhou, and J. Lu, “Tri-perspective view for vision-based 3d semantic occupancy prediction,” in *Proceedings of the IEEE/CVF Conference on Computer Vision and Pattern Recognition (CVPR)*, June 2023, pp. 9223–9232.

[48] Y. Huang, W. Zheng, B. Zhang, J. Zhou, and J. Lu, “Selfocc: Self-supervised vision-based 3d occupancy prediction,” in *Proceedings of the IEEE/CVF Conference on Computer Vision and Pattern Recognition (CVPR)*, June 2024, pp. 19946–19956.

[49] M. Pan, J. Liu, R. Zhang, P. Huang, X. Li, H. Xie, B. Wang, L. Liu, and S. Zhang, “Renderocc: Vision-centric 3d occupancy prediction with 2d rendering supervision,” in *2024 IEEE International Conference on Robotics and Automation (ICRA)*, 2024, pp. 12404–12411.

[50] Y. Huang, W. Zheng, Y. Zhang, J. Zhou, and J. Lu, “Gaussianformer: Scene as gaussians for vision-based 3d semantic occupancy prediction,” in *European Conference on Computer Vision*. Springer, 2024, pp. 376–393.

[51] Y. Huang, A. Thammatakrakoon, W. Zheng, Y. Zhang, D. Du, and J. Lu, “Gaussianformer-2: Probabilistic gaussian superposition for efficient 3d occupancy prediction,” in *Proceedings of the Computer Vision and Pattern Recognition Conference*, 2025, pp. 27477–27486.

[52] W. Gan, F. Liu, H. Xu, N. Mo, and N. Yokoya, “Gaussianocc: Fully self-supervised and efficient 3d occupancy estimation with gaussian splatting,” in *Proceedings of the IEEE/CVF International Conference on Computer Vision*, 2025, pp. 28980–28990.

[53] Z. Zhu, S. Wang, J. Xie, J.-j. Liu, J. Wang, and J. Yang, “Voxelsplat: Dynamic gaussian splatting as an effective loss for occupancy and flow prediction,” in *Proceedings of the Computer Vision and Pattern Recognition Conference*, 2025, pp. 6761–6771.

[54] J. Ma, X. Chen, J. Huang, J. Xu, Z. Luo, J. Xu, W. Gu, R. Ai, and H. Wang, “Cam4docc: Benchmark for camera-only 4d occupancy forecasting in autonomous driving applications,” in *Proceedings of the IEEE/CVF Conference on Computer Vision and Pattern Recognition (CVPR)*, June 2024, pp. 21486–21495.

[55] L. Wang, W. Zheng, Y. Ren, H. Jiang, Z. Cui, H. Yu, and J. Lu, “Occsora: 4d occupancy generation models as world simulators for autonomous driving,” 2024.

[56] N. Singla, “Motion detection based on frame difference method,” *International Journal of Information & Computation Technology*, vol. 4, no. 15, pp. 1559–1565, 2014.

[57] H. Caesar, V. Bankiti, A. H. Lang, S. Vora, V. E. Liou, Q. Xu, A. Krishnan, Y. Pan, G. Baldan, and O. Beijbom, “nuscenes: A multi-modal dataset for autonomous driving,” in *Proceedings of the IEEE/CVF Conference on Computer Vision and Pattern Recognition (CVPR)*, June 2020.

[58] I. Goodfellow, “Deep learning,” 2016.

[59] J. Long, E. Shelhamer, and T. Darrell, “Fully convolutional networks for semantic segmentation,” in *Proceedings of the IEEE Conference on Computer Vision and Pattern Recognition (CVPR)*, June 2015.

[60] T. N. Kipf and M. Welling, “Semi-supervised classification with graph convolutional networks,” 2017.

[61] T.-Y. Lin, P. Goyal, R. Girshick, K. He, and P. Dollár, “Focal loss for dense object detection,” in *Proceedings of the IEEE international conference on computer vision*, 2017, pp. 2980–2988.

[62] M. Berman, A. R. Triki, and M. B. Blaschko, “The lovász-softmax loss: A tractable surrogate for the optimization of the intersection-over-union measure in neural networks,” in *Proceedings of the IEEE conference on computer vision and pattern recognition*, 2018, pp. 4413–4421.

[63] G. Farnebäck, “Two-frame motion estimation based on polynomial expansion,” in *Image Analysis*, J. Bigun and T. Gustavsson, Eds. Berlin, Heidelberg: Springer Berlin Heidelberg, 2003, pp. 363–370.

[64] M. Everingham, L. van Gool, C. Williams, J. Winn, and A. Zisserman, “The pascal visual object classes (voc) challenge,” *International Journal of Computer Vision*, vol. 88, no. 2, pp. 303–338, Jun. 2010.

[65] T.-Y. Lin, M. Maire, S. Belongie, J. Hays, P. Perona, D. Ramanan, P. Dollár, and C. L. Zitnick, “Microsoft coco: Common objects in context,” in *Computer Vision – ECCV 2014*, D. Fleet, T. Pajdla, B. Schiele, and T. Tuytelaars, Eds. Cham: Springer International Publishing, 2014, pp. 740–755.

[66] M. Cordts, M. Omran, S. Ramos, T. Rehfeld, M. Enzweiler, R. Benenson, U. Franke, S. Roth, and B. Schiele, “The cityscapes dataset for semantic urban scene understanding,” in *Proceedings of the IEEE Conference on Computer Vision and Pattern Recognition (CVPR)*, June 2016.

[67] K. He, G. Gkioxari, P. Dollar, and R. Girshick, “Mask r-cnn,” in *Proceedings of the IEEE International Conference on Computer Vision (ICCV)*, Oct 2017.

[68] Z. Murez, T. van As, J. Bartolozzi, A. Sinha, V. Badrinarayanan, and A. Rabinovich, “Atlas: End-to-end 3d scene reconstruction from posed images,” in *Computer Vision – ECCV 2020*, Cham, 2020, pp. 414–431.

[69] Z. Li, W. Wang, H. Li, E. Xie, C. Sima, T. Lu, Y. Qiao, and J. Dai, “Bevformer: Learning bird’s-eye-view representation from multi-camera images via spatiotemporal transformers,” in *Computer Vision – ECCV 2022*. Cham: Springer Nature Switzerland, 2022, pp. 1–18.



Fengcheng Yu received a bachelor’s degree in engineering from the School of Intelligent Engineering of Sun Yat-sen University, majoring in intelligent science and technology, 2025. He is currently pursuing the MS in Computer Science degree with the Viterbi School of Engineering, University of Southern California, California, USA.

His research interests includes autonomous driving, high performance computing.



Haoran Xu received the master’s degree in Software Engineering from Guangdong University of Technology, Guangzhou, China, in 2022. He is currently pursuing the Ph.D. degree with the School of Intelligent Systems Engineering, Sun Yat-Sen University, Shenzhen, China, and also with Peng Cheng Laboratory, Shenzhen, China.

His research interests include multi-agent systems, reinforcement learning, and their applications in connected and autonomous vehicles.



Canming Xia received the master’s degree in Control Science and Engineering from Guangdong University of Technology, Guangzhou, China, in 2023. Presently, He is pursuing the Ph.D. degree with the School of Intelligent Systems Engineering, Sun Yat-Sen University, Shenzhen, China.

His research interests include decision for autonomous vehicles, reinforcement learning, and representation learning.



Ziyang Zong received the master's degree in Computer Science and Technology from Nanjing University of Information Science and Technology, Nanjing, China, in 2023. Presently, she is pursuing the Ph.D. degree with the School of Intelligent Systems Engineering, Sun Yat-Sen University, Shenzhen, China.

Her research interests include domain adaptation, 3D-generation, and representation learning.



Guang Tan (Member, IEEE) received the Ph.D. degree in computer science from the University of Warwick, Coventry, U.K., in 2007

He was a Professor with the Shenzhen Institutes of Advanced Technology, Chinese Academy of Sciences, Shenzhen, China. He has been a Professor with the School of Intelligent Systems Engineering, Sun Yat-sen University, Guangzhou, China, since 2018, where he works on networked systems and machine learning.